IEEE Access
Multidisciplinary ⋮ Rapid Review ⋮ Open Access Journal

Received November 5, 2020, accepted November 13, 2020, date of publication November 17, 2020,
date of current version November 30, 2020.

Digital Object Identifier 10.1109/ACCESS.2020.3038656

Improved Differential Evolution Algorithm for Multi-Target Response Inversion Detected by a Portable Transient Electromagnetic Sensor

SHUDONG CHEN[1], SHUANG ZHANG[1], XINQUN LUAN[2], AND ZHAOHE LIU[2]
[1]College of Electronic Science and Engineering, Jilin University, Changchun 130012, China
[2]Science and Technology on Near-Surface Detection Laboratory, Wuxi 214035, China

Corresponding authors: Shuang Zhang (zhangshuang@jlu.edu.cn) and Zhaohe Liu (lzhh@vip.sina.com)

This work was supported in part by the National Natural Science Foundation of China under Grant 41704145, and in part by the Foundation of Science and Technology on Near-Surface Detection Laboratory under Grant 6142414060111.

ABSTRACT The superimposed response of multi-target causes difficulty in locating and characterizing each target when detecting unexploded ordnance with a portable transient electromagnetic sensor, constructed with a single-layer transmitting coil and five three-component receiving coils. Differential evolution (DE) algorithm is improved here with Gram–Schmidt orthogonalization and position rearrangement for superimposed response inversion based on the multisource model, which represents the multi-target response with a set of magnetic dipoles distributed over the interrogated area. The Gram–Schmidt orthogonalization turns the coefficient matrix of each target into an orthonormal basis. Accordingly, the best magnetic polarization tensor can be directly extracted from the superimposed response without inverting large and potentially ill-conditioned matrices. The position rearrangement groups the positions of individuals in the contemporary population to maximize the likelihood that the positions in the same group belong to the same target. The convergence speed of multi-target inversion is accelerated with the crossover operation of DE algorithm performed within the groups. Simulated experiment results show that the error in estimated position and characteristic response for improved DE algorithm is only 10% of that of the conventional DE algorithm. Field experiment is also conducted, and its results show that the error in estimated position for improved DE algorithm is only 20% of that of the conventional DE algorithm. The improved DE algorithm can accurately estimate the position and characteristic response of each target from superimposed response.

INDEX TERMS Unexploded ordnance, portable transient electromagnetic sensor, differential evolution algorithm, Gram–Schmidt orthogonalization, multisource model.

I. INTRODUCTION

As an increasingly serious international humanitarian and environmental problem worldwide, unexploded ordnance (UXO) in former battlefields and decommissioned firing ranges prevents land use, threatens public safety, and causes hundreds of victims each year [1], [2]. The clearance of subsurface UXOs mixed with a large number of harmless objects is usually a dangerous, slow, and costly process. The most important thing in the cleaning of UXOs is not detection but accurately distinguishing UXOs from harmless targets [3].

Various geophysical methods are used for UXO detection in recent years [4], [5]. Magnetic detection [6], [7], electromagnetic induction (EMI) [8], [9], and ground-penetrating radar [10]–[12] have been the main geophysical methods. EM sensors in high frequencies have been widely used for direction of arrival estimation [13]–[15]. In low frequencies, ranging from tens to a few hundreds of kilohertz, at which the ground is essentially transparent, the EM sensors are considered a promising method in underground target detection. Transient electromagnetic (TEM) sensing, which is a time-domain EMI method, has been found to be effective in detecting and discriminating UXOs.

Detection, inversion, and classification are three main stages in cleaning UXOs with a TEM system. In the first stage, different systems are used to detect the underground target for determining whether a UXO-like target exists. All systems, such as the airborne system [16], the vehicle

The associate editor coordinating the review of this manuscript and approving it for publication was Baoping Cai.

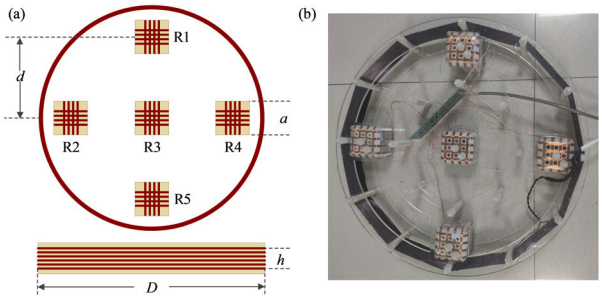

FIGURE 1. (a) Physical model of the sensor; (b) picture of the sensor.

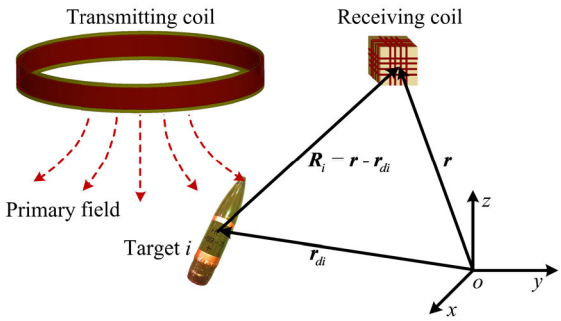

FIGURE 2. Operation principle of TEM detection and multisource model.

TABLE 1. Parameters of the portable sensor.

Coils	Parameters	Symbol	Value
Transmitting coil	Diameter (cm)	D	50
	Height (cm)	h	7
	Number of turns	n_T	30
	Resistance (Ω)	r_T	0.9
	Inductance (μH)	L_T	790
Receiving coil	Length (cm)	a	5.6
	Distance between coils (cm)	d	20
	Inductance (mH)	L	42.6
	Resistance (Ω)	r	166
	Self-capacitance (pF)	C	120

systems [17]–[19], and the portable systems [20]–[23], have been developed to increase detection probability for targets in different depths. In the final stage, different algorithms, such as maximum-likelihood methods, mixed models, and support vector machines [24]–[27], have been used to determine whether the underground target is a dangerous UXO or a harmless clutter. Between detection and classification, the inversion recovers a set of parameters based on a physics-based model.

The single dipole approximation has been the most frequently used model to represent the target response for speed and simplicity. However, this model reduces the underground targets to a point and assumes the primary field uniform throughout the target regardless of the volume, structure, and distribution of the targets. The model will break down for a single target with large volume [23], [28] and complicated structure or multiple targets. A multisource model may provide a better description in these situations. Inversion of target response based on the multisource model is mostly conducted with the vehicle system, such as MetalMapper [17], or the Time-Domain Electromagnetic Multisensor Towed Array Detection System [19]. The joint diagonalization [29], [30], the orthonormalized volume magnetic source model [30]–[32], the multiple signal classification algorithm [33], [34], and some other algorithms [35]–[37] have been applied for multisource inversion.

However, the vehicle system is too large and heavy and cannot be readily used in rough or tree-covered terrains. The portable system can work in various complex conditions. The portable TEM sensor, which is constructed with a transmitting coil and five three-component receiving coils, cannot provide measurements with very rich information as vehicle system. Inversion algorithms for the vehicle system cannot be directly applied for the portable system. Thus, an improved differential evolution (DE) algorithm is developed here on the basis of the multisource model to invert the multi-target response detected by the portable TEM system.

The rest of the paper is organized as follows. First, the structure and parameters of the portable sensor are presented. Then, the multisource model and improved DE algorithm is discussed in detail. The performance of the improved DE algorithm is verified by the simulated data. Finally, the field experiments are performed to locate and characterize the multi-target with the improved DE algorithm for portable TEM system.

II. SENSOR OF THE PORTABLE SYSTEM

Figure 1 shows the physical model and the picture of the portable TEM sensor. The receiving coil in this manuscript is new designed to record the late time response for a better recognition of target. The sensor is composed of one single-layer transmitting coil wrapped around a round framework and five three-component receiving coils wound on the square framework. The diameter and height of the transmitting coil are D and h. The length of five three-component receiving coils numbered as R1, R2, R3, R4, and R5 is a, and the distance between the two nearby receiving coils is d. Table 1 provides a list of the specifications of the portable sensor.

The period, duty cycle, and amplitude of the bipolar trapezoidal current in transmitting coil are 80 ms, 50%, and 7.5 A, respectively. The switch-off time of transmitting current is approximately 60 μs.

III. RESPONSE INVERSION

A. MULTISOURCE MODEL

The pulsed primary field $\boldsymbol{B}_P$ generated by transmitting coil will induce the eddy current inside the conductive and permeability target, which produces a secondary field $\boldsymbol{B}_S$ that slowly decays over time. The single target is usually modeled by a magnetic dipole when it is sufficiently small or far from the sensor. The multi-target response can be represented with

a multisource model. Figure 2 presents the operation principle of TEM detection and the multisource model.

In Figure 2, the secondary field $\boldsymbol{B}_{\mathrm{S}i}$ of i-th target at the position of receiving coil $\boldsymbol{r}$ is given by [30]

$$\boldsymbol{B}_{Si} = \frac{(3\boldsymbol{e}_{Ri}\boldsymbol{e}_{Ri} - \mathbf{I})\,\boldsymbol{m}_i}{4\pi R_i^3} = \boldsymbol{G}(\boldsymbol{R}_i)\,\boldsymbol{m}_i, \tag{1}$$

where $\boldsymbol{e}_{Ri}$ represents the unit vector along the relative position vector $\boldsymbol{R_i} = \boldsymbol{r} - \boldsymbol{r_{di}}$, $\boldsymbol{r_{di}}$ is the position of the i-th target, R_i denotes the modulus of $\boldsymbol{R}_i$, and $\mathbf{I}$ represents the identity matrix. $\boldsymbol{G}(\boldsymbol{R}_i)$ is the Green's function of receiving coils. The dipole moment $\boldsymbol{m}_i$ of the i-th target can be calculated as

$$\boldsymbol{m}_i = \boldsymbol{M}_i\boldsymbol{B}_P(\boldsymbol{r}_{di}), \tag{2}$$

where $\boldsymbol{M}_i$, the magnetic polarizability tensor (MPT) of the i-th target, is a 3×3 symmetric matrix; which depends on the target's shape, size, orientation, and material properties. $\boldsymbol{B}_{\mathrm{P}}(\boldsymbol{r}_{di})$ is the primary field throughout the i-th target.

According to Faraday's law of EMI, the target response $\boldsymbol{V}_i$ of an EMI system is proportional to the derivative of the secondary field $\boldsymbol{B}_{\mathrm{S}i}$, which is given by

$$\boldsymbol{V}_i = -\boldsymbol{G}(\boldsymbol{R}_i)\frac{d\boldsymbol{M}_i}{dt}\boldsymbol{B}_P(\boldsymbol{r}_{di}) = \boldsymbol{G}(\boldsymbol{R}_i)\,\boldsymbol{L}_i(t)\boldsymbol{B}_P(\boldsymbol{r}_{di}), \tag{3}$$

where the characteristic matrix $\boldsymbol{L}_i(t)$ is defined as the negative derivative of MPT, and t is the time.

According to Equation 3, the response of a buried target can be decomposed into two parts: a nonlinear part consisting of only the target position $\boldsymbol{r}_{di}$ and a linear part consisting of the target characteristic vector $\boldsymbol{p}_i(t)$ [23], [30].

$$\boldsymbol{V}_i = \boldsymbol{\gamma}(\boldsymbol{r}_{di})\,\boldsymbol{p}_i(t), \tag{4}$$

where $\boldsymbol{p}_i(t)$ is a 6×1 dimensional vector with components $(L_{ixx}, L_{ixy}, L_{ixz}, L_{iyy}, L_{iyz}, L_{izz})$ that correspond to the elements of the target characteristic matrix $\boldsymbol{L}_i(t)$. $\boldsymbol{\gamma}(\boldsymbol{r}_{di})$ is a 15×6 matrix, which is only dependent on the target position $\boldsymbol{r}_{di}$.

Equation (4) represents the response of the i-th target under a single excitation of the portable system. When conducting detection with the portable system, the target is excited by a primary field generated at N different positions. The responses of the i-th target $\boldsymbol{V}_i$ can be given by

$$\boldsymbol{V}_i = \begin{bmatrix} \boldsymbol{V}_{i1} \\ \vdots \\ \boldsymbol{V}_{iN} \end{bmatrix} = \begin{bmatrix} \boldsymbol{\gamma}_{i1} \\ \vdots \\ \boldsymbol{\gamma}_{iN} \end{bmatrix} \boldsymbol{p}_i(t) = \boldsymbol{\gamma}(\boldsymbol{r}_{di})\,\boldsymbol{p}_i(t), \tag{5}$$

where $\boldsymbol{V}_i$ is a $15N \times 1$ dimensional vector and $\boldsymbol{\gamma}(\boldsymbol{r}_{di})$ is a $15N \times 6$ matrix, which is only dependent on the target position $\boldsymbol{r}_{di}$.

The response of multi-target can be expressed as a superposition of all individual responses. When the number of targets is T, the positions of these targets are $\boldsymbol{r}_{d1}, \boldsymbol{r}_{d2}, \ldots, \boldsymbol{r}_{dT}$, and the characteristic vectors of corresponding targets are $\boldsymbol{p}_1(t)$, $\boldsymbol{p}_2(t), \ldots, \boldsymbol{p}_{\mathrm{T}}(t)$. The response can be expressed as

$$\boldsymbol{V} = \begin{bmatrix} \boldsymbol{\gamma}(\boldsymbol{r}_{d1}) & \ldots & \boldsymbol{\gamma}(\boldsymbol{r}_{dT}) \end{bmatrix} \begin{bmatrix} \boldsymbol{p}_1(t) \\ \vdots \\ \boldsymbol{p}_T(t) \end{bmatrix} = \boldsymbol{\gamma}\boldsymbol{p}. \tag{6}$$

where $\boldsymbol{\gamma}$ is the coefficient matrix of the multi-target response and $\boldsymbol{p}$ is the characteristic vector of multi-target.

The number of sources T is usually unknown, and we can consider it a variety of an optimization routine. However, this topic is outside the scope of this study.

B. MULTISOURCE INVERSION

On the basis of the forward model established by Equation (6), the parameters of all buried targets, which consist of positions and the characteristic vectors, can be estimated by defining an objective function ϕ that quantifies the goodness-of-fit between the measured data $\boldsymbol{V}_{\mathrm{obs}}$ and the predictions of the forward model. The least square approach is used to recover the parameters as

$$\min \phi = \|\boldsymbol{V}_{obs} - \boldsymbol{\gamma}\boldsymbol{p}\|^2. \tag{7}$$

where, $\|\ \|$ denotes the norm if a vector.

Conventionally, the coefficient matrix $\boldsymbol{\gamma}$ is first calculated with the initial positions $(\boldsymbol{r}_{\mathrm{d}10}, \boldsymbol{r}_{\mathrm{d}10} \ldots \boldsymbol{r}_{\mathrm{dT}0})$. Then, the corresponding characteristic vector $\boldsymbol{p}$ is calculated by matrix inversion. The positions and characteristic vectors can be finally estimated by optimizing the target positions with selection, mutation, and crossover of DE algorithm [38]. The conventional DE algorithm can accurately estimate the position and characteristic response of a single target. Different from single dipole inversion, inversion of multisource model faces two problems.

First, the dimensionality of the γ matrix increases with the number of targets. This condition results in a rapid increase in the amount of computation of the characteristic vector $\boldsymbol{p}(t)$ and the need to invert large and potentially ill-conditioned matrices. The conventional DE algorithm can achieve the lowest overall objective function ϕ between measured data $\boldsymbol{V}_{\mathrm{obs}}$ and forward model. However, it cannot guarantee that the estimated characteristic vector for each target is the most suitable. The Gram–Schmidt orthogonalization is introduced to solve the problem.

Second, the position of the single dipole inversion is definite, which can be quickly converged through iteration. In multisource inversion process, the positions of different targets can be combined in different orders. Thus, the DE algorithm does not have a definite convergence value, which will cause the algorithm to converge slowly. The position rearrangement is proposed to improve the convergence speed.

An improved DE algorithm with the Gram–Schmidt orthogonalization and position rearrangement based on the multisource model is proposed here. The flowchart of the improved DE algorithm is shown in Figure 3. Three core steps are involved in the improved DE algorithm. First, the cost function ϕ is calculated by the Gram–Schmidt orthogonalization. Second, target position and characteristic vector are estimated with position rearrangement in the improved DE algorithm. Third, the characteristic response is calculated with singular value decomposition (SVD).

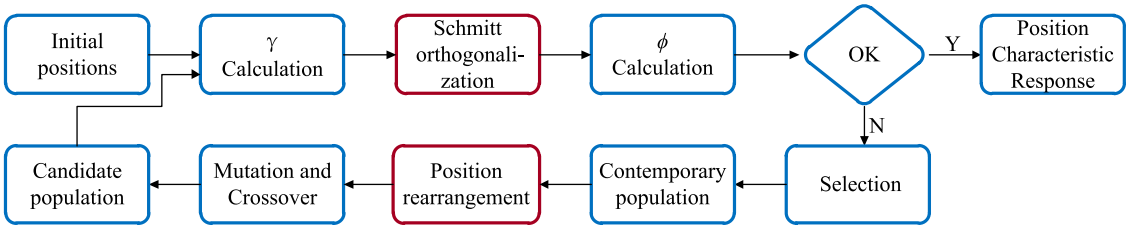

FIGURE 3. Flowchart of the improved DE algorithm based on the multisource model.

1) GRAM–SCHMIDT ORTHOGONALIZATION

The orthogonalization inversion method configures the optimal characteristic vector $\boldsymbol{p}_i(t)$ for each coefficient matrix $\gamma(\boldsymbol{r}_{di})$. The response of multi-target $\boldsymbol{V}$ is expressed as a linear combination of a set of orthogonal vectors $\boldsymbol{b}_i(t)$ according to Equation (6):

$$\boldsymbol{V} = \boldsymbol{\gamma p} = \sum_{i=1}^{T} \boldsymbol{\gamma}\left(\boldsymbol{r}_{di}\right)\boldsymbol{p}_i\left(t\right) = \sum_{i=1}^{T} \boldsymbol{\Psi}_i \boldsymbol{b}_i\left(t\right). \tag{8}$$

The coefficient matrices $\boldsymbol{\Psi}_i$ are orthogonal to each other, and the inner product of two identical $\boldsymbol{\Psi}_i$ matrices is defined as $\boldsymbol{F}_i$:

$$\boldsymbol{\Psi}'_i\boldsymbol{\Psi}_j = \boldsymbol{0}, \quad i \neq j,\ \boldsymbol{\Psi}'_i\boldsymbol{\Psi}_i = \boldsymbol{F}_i. \tag{9}$$

The Gram–Schmidt orthogonalization method is used to calculate the coefficient matrix $\boldsymbol{\Psi}_i$.

$$\begin{aligned} \boldsymbol{\Psi}_1 &= \boldsymbol{\gamma}_1, \\ &\cdots \\ \boldsymbol{\Psi}_i &= \boldsymbol{\gamma}_i - \sum_{k=1}^{i-1} \boldsymbol{\Psi}_k \boldsymbol{A}_{ki}, \\ &\cdots \\ \boldsymbol{\Psi}_T &= \boldsymbol{\gamma}_T - \sum_{k=1}^{T-1} \boldsymbol{\Psi}_k \boldsymbol{A}_{kT}. \end{aligned} \tag{10}$$

The coefficient $\boldsymbol{A}_{ki}$ can be calculated as follows:

$$\begin{aligned} \boldsymbol{A}_{11} &= 1, \\ &\cdots \\ \boldsymbol{A}_{ij} &= \boldsymbol{F}_i^{-1}\left(\boldsymbol{\Psi}'_i\boldsymbol{\gamma}_j\right), \\ &\cdots \\ \boldsymbol{A}_{TT} &= 1. \end{aligned} \tag{11}$$

Equations (10) and (11) show that Gram–Schmidt orthogonalization is a progressive process. First, the matrix $\boldsymbol{\gamma}_1$ of the first target is calculated according to Equations (3) and (4). Then, the coefficient $\boldsymbol{A}_{11}$ and the first orthogonal component $\boldsymbol{\Psi}_1$ are calculated according to Equations (10) and (11). Next, the components of the coefficient matrix $\boldsymbol{\Psi}_1$ in the $\boldsymbol{\gamma}_2$ to $\boldsymbol{\gamma}_\mathrm{T}$ need to be calculated according to Equations (10) and (11) to obtain the coefficient $\boldsymbol{A}_{21}$ to $\boldsymbol{A}_{2\mathrm{T}}$ and the matrix $\boldsymbol{\Psi}_2$. The components of the coefficient matrix $\boldsymbol{\Psi}_2$ in the $\boldsymbol{\gamma}_3$ to $\boldsymbol{\gamma}_\mathrm{T}$ can be calculated to obtain the coefficient $\boldsymbol{A}_{31}$ to $\boldsymbol{A}_{3\mathrm{T}}$ and the matrix $\boldsymbol{\Psi}_3$. All coefficients $\boldsymbol{A}_{ij}$ and orthogonal components $\boldsymbol{\Psi}_\mathrm{i}$ are finally obtained.

The characteristic vector $\boldsymbol{b}_i(t)$ can be calculated by Equations (8) and (9), that is,

$$\boldsymbol{b}_i = \boldsymbol{F}_i^{-1}\left(\boldsymbol{\Psi}'_i\boldsymbol{V}\right). \tag{12}$$

Equation (12) shows that only a 6×6 matrix $\boldsymbol{F}_i$ needs to be inverted to obtain the corresponding characteristic vector $\boldsymbol{b}_i$ under orthogonal conditions. Accordingly, the magnetic polarization tensor can be directly extracted from the measured superimposed response without inverting large and potentially ill-conditioned matrices. Meanwhile, orthogonal operation can effectively suppress the noise and improve the accuracy of inversion results.

Once the orthogonal $\boldsymbol{\Psi}_i$ matrixes and corresponding characteristic vector $\boldsymbol{b}_i(t)$ are obtained, the objective function ϕ can be directly calculated according to Equations (7) and (8).

$$\phi\left(\boldsymbol{v}\right) = \left\| \boldsymbol{V}_{\boldsymbol{obs}} - \sum_{i=1}^{T} \gamma\left(\boldsymbol{r}_{di}\right)\boldsymbol{p}_i\left(t\right) \right\|^2 = \left\| \boldsymbol{V}_{\boldsymbol{obs}} - \sum_{i=1}^{T} \Psi_i \boldsymbol{b}_i\left(t\right) \right\|^2. \tag{13}$$

As shown in Equations (8)–(13), the orthogonal $\boldsymbol{\Psi}_i$ matrix and the corresponding characteristic vector $\boldsymbol{b}_i$ can be quickly and accurately calculated by the Gram–Schmidt orthogonalization. The cost function ϕ can be directly calculated with the orthogonal $\boldsymbol{\Psi}_i$ matrix and the corresponding characteristic vector $\boldsymbol{b}_i$. This method greatly accelerates the inversion speed and improves the inversion accuracy.

2) POSITION REARRANGEMENT

The conventional DE algorithm generates candidate populations by mutation and crossover of contemporary population. Then, the algorithm calculates the cost function ϕ of the candidate population. The next generation is selected by comparing the cost functions ϕ of the candidate and contemporary populations. In multisource inversion, this process becomes extremely complicated.

In the dual-target DE inversion, the true value of the position vector $\boldsymbol{v}$ is $(\boldsymbol{r}_{d1}, \boldsymbol{r}_{d2})$ and the number of individuals in the population is K. In the evolution process, the population of the G-th generation can be expressed as $\{(\boldsymbol{r}_{d1G1}, \boldsymbol{r}_{d2G1}), \ldots, (\boldsymbol{r}_{d1GK}, \boldsymbol{r}_{d2GK})\}$. Candidate populations can be generated by the crossover of contemporary populations as

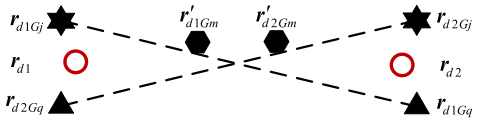

FIGURE 4. Crossover of dual-target for conventional DE algorithm.

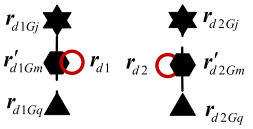

FIGURE 5. Crossover of dual-target for improved DE algorithm.

[38]

$$\left(\boldsymbol{r}'_{d1Gm}, \boldsymbol{r}'_{d2Gm}\right) = \boldsymbol{k}\left(\boldsymbol{r}_{d1Gj}, \boldsymbol{r}_{d2Gj}\right) + (1-k)\left(\boldsymbol{r}_{d1Gq}, \boldsymbol{r}_{d2Gq}\right), \tag{14}$$

where $(\boldsymbol{r}'_{d1Gm}, \boldsymbol{r}'_{d2Gm})$ is the m-th individual of candidate populations; $(\boldsymbol{r}_{d1Gj}, \boldsymbol{r}_{d2Gj})$ and $(\boldsymbol{r}_{d1Gq}, \boldsymbol{r}_{d2Gq})$ are individuals in the contemporary population; j and q are two random integers between 1 and K; and k is a crossover factor between 0 and 1. Figure 4 describes the process.

As shown in Figure 4, individuals $(\boldsymbol{r}_{d1Gj}, \boldsymbol{r}_{d2Gj})$ and $(\boldsymbol{r}_{d1Gq}, \boldsymbol{r}_{d2Gq})$ in the G-th generation are close to $(\boldsymbol{r}_{d1}, \boldsymbol{r}_{d2})$ and $(\boldsymbol{r}_{d2}, \boldsymbol{r}_{d1})$, respectively. The corresponding cost function of these individuals is very small. However, the candidate individual $(\boldsymbol{r}'_{d1Gm}, \boldsymbol{r}'_{d2Gm})$ generated by the individuals $(\boldsymbol{r}_{d1Gj}, \boldsymbol{r}_{d2Gj})$ and $(\boldsymbol{r}_{d1Gq}, \boldsymbol{r}_{d2Gq})$ locates between $(\boldsymbol{r}_{d1}, \boldsymbol{r}_{d2})$ and $(\boldsymbol{r}_{d2}, \boldsymbol{r}_{d1})$. The cost function of candidate individual $(\boldsymbol{r}'_{d1Gm}, \boldsymbol{r}'_{d2Gm})$ is much greater than that of individuals $(\boldsymbol{r}_{d1Gj}, \boldsymbol{r}_{d2Gj})$ and $(\boldsymbol{r}_{d1Gq}, \boldsymbol{r}_{d2Gq})$. Crossover operations on two random individuals in the contemporary population do not result in good evolution of the population. When the number of targets T is large, the crossover operation will be more complicated, and the algorithm will converge much slower.

In this process, the cost function ϕ of both individuals in the contemporary population is very low. However, the convergence goals are not the same: one is $(\boldsymbol{r}_{d1}, \boldsymbol{r}_{d2})$, and the other is $(\boldsymbol{r}_{d2}, \boldsymbol{r}_{d1})$. This condition directly leads to a worse convergence of the candidate group. The position rearrangement is adopted to solve this problem. The steps of position rearrangement are described as follows:

(1) Find the individual with the smallest cost function in the contemporary population.

(2) Adjust the order of target position for other individuals in the contemporary population to obtain a set of position vectors.

(3) Calculate the distance between each position vector of the individual and the one with the minimum cost function.

(4) Select the position vector with the smallest distance to replace the original position vector for each individual in contemporary population.

After position rearrangement, the crossover operation can effectively accelerate the convergence speed, as shown in Figure 5. The individual $(\boldsymbol{r}_{d1Gq}, \boldsymbol{r}_{d2Gq})$ is reordered after rearrangement, which makes it closer to $(\boldsymbol{r}_{d1}, \boldsymbol{r}_{d2})$. Thus, the distance between $(\boldsymbol{r}_{d1}, \boldsymbol{r}_{d2})$ and the candidate population (r'_{d1Gm}, r'_{d2Gm}) generated by the individuals (r_{d1Gj}, r_{d2Gj}) and (r_{d1Gq}, r_{d2Gq}) in the G-th generation population may be much closer. This process regroups the positions of individuals to maximize the likelihood that the positions in the same group belong to the same target. Accordingly, cross-operation of two rearranged individuals in the contemporary population can result in the good evolutionary effect of the population and will cause faster convergence of the algorithm.

3) TARGET CHARACTERIZATION

With the Gram–Schmidt orthogonalization and position rearrangement proposed above, the improved DE algorithm is applied to accurately estimate the target position and characteristic vector. According to Equations (8)–(11), the relationship between the coefficient matrixes $\boldsymbol{\gamma}$ and Ψ and the coefficient $\boldsymbol{A}_{ij}$ can be represented in the form of the matrix.

$$\begin{bmatrix}\boldsymbol{\gamma}_1 & \boldsymbol{\gamma}_2 & \cdots & \boldsymbol{\gamma}_T\end{bmatrix} = \begin{bmatrix}\boldsymbol{\Psi}_1 & \boldsymbol{\Psi}_2 & \ldots & \boldsymbol{\Psi}_T\end{bmatrix} \begin{bmatrix} 1 & \boldsymbol{A}_{12} & \ldots & \boldsymbol{A}_{1T} \\ 0 & 1 & \ldots & \boldsymbol{A}_{2T} \\ \ldots & \ldots & \ldots & \ldots \\ 0 & 0 & \ldots & 1 \end{bmatrix}. \tag{15}$$

According to Equations (8) and (15), the relationship between the characteristic vector $\boldsymbol{b}_i(t)$ and $\boldsymbol{p}_i(t)$ can be obtained as

$$\begin{bmatrix}\boldsymbol{b}_1 \\ \boldsymbol{b}_2 \\ \ldots \\ \boldsymbol{b}_T\end{bmatrix} = \begin{bmatrix} 1 & \boldsymbol{A}_{12} & \ldots & \boldsymbol{A}_{1T} \\ 0 & 1 & \ldots & \boldsymbol{A}_{2T} \\ \ldots & \ldots & \ldots & \ldots \\ 0 & 0 & \ldots & 1 \end{bmatrix} \begin{bmatrix}\boldsymbol{p}_1 \\ \boldsymbol{p}_2 \\ \ldots \\ \boldsymbol{p}_T\end{bmatrix}. \tag{16}$$

The characteristic vector $\boldsymbol{p}_i(t)$ can be calculated with the characteristic vector $\boldsymbol{b}_i(t)$.

$$\begin{bmatrix}\boldsymbol{p}_1 \\ \boldsymbol{p}_2 \\ \ldots \\ \boldsymbol{p}_T\end{bmatrix} = \begin{bmatrix} 1 & \boldsymbol{B}_{12} & \ldots & \boldsymbol{B}_{1T} \\ 0 & 1 & \ldots & \boldsymbol{B}_{2T} \\ \ldots & \ldots & \ldots & \ldots \\ 0 & 0 & \ldots & 1 \end{bmatrix} \begin{bmatrix}\boldsymbol{b}_1 \\ \boldsymbol{b}_2 \\ \ldots \\ \boldsymbol{b}_T\end{bmatrix}. \tag{17}$$

The matrix element $\boldsymbol{B}_{ij}$ can be calculated as follows:

$$\begin{aligned} \boldsymbol{B}_{mm} &= I, \\ \boldsymbol{B}_{(m-1)m} &= -\boldsymbol{A}_{(m-1)m}, \\ \boldsymbol{B}_{qm} &= -\sum_{l=q}^{m-1} \boldsymbol{B}_{ql}\boldsymbol{A}_{lm}, \quad 1 \le q \le m-2. \end{aligned} \tag{18}$$

When the matrix element $\boldsymbol{B}_{ij}$ is calculated, the characteristic vector $\boldsymbol{p}_i(t)$ corresponding to each target can be directly calculated according to Equations (17) and (18).

When the characteristic vector $\boldsymbol{p}_i(t)$ is finally estimated, the characteristic matrix $\boldsymbol{L}_i(t)$ of the target can be rebuilt. The principal polarizability elements of the characteristic matrix $\boldsymbol{L}_i(t)$ can be calculated using SVD, as follows:

$$\boldsymbol{L}_i(t) = \boldsymbol{U}_i \begin{bmatrix} l_{pi}(t) & 0 & 0 \\ 0 & l_{v1i}(t) & 0 \\ 0 & 0 & l_{v2i}(t) \end{bmatrix} \boldsymbol{U}'_i, \tag{19}$$

where $l_{v1i}(t)$ and $l_{v2i}(t)$ indicate the principal polarizability elements perpendicular to the symmetry axis of the target. $l_{pi}(t)$ is the principal polarizability element parallel to the symmetry axis of the target. For axisymmetric targets, $l_{v1i}(t)$ and $l_{v2i}(t)$ are equal, and defined as $l_{vi}(t)$.

The principal polarizability elements of the characteristic matrix $l_{pi}(t)$, $l_{v1i}(t)$, and $l_{v2i}(t)$ are defined as the characteristic response $\boldsymbol{l}_i(t)$ of a target.

$$\boldsymbol{l}_i(t) = \begin{bmatrix} l_{pi}(t) & l_{v1i}(t) & l_{v2i}(t) \end{bmatrix}. \tag{20}$$

With the target position $\boldsymbol{r}_{di}$ and the characteristic response $\boldsymbol{l}_i(t)$ estimated, the location and characterization of a target are realized. In the next section, the location and characterization of multiple targets with the portable TEM system with by conventional DE algorithm and improved DE algorithm are discussed in detail.

IV. SIMULATION

In this section, we present results of numerical experiment to compare the performance of the conventional and improved DE algorithms for multi-target location and characterization. The response of three targets A, B, and C are calculated on the basis of the multisource model described in Equation (6) for the portable TEM system. Figure 6 depicts the setup and simulated response added with noise.

As shown in Figure 6(a), the measurement area is 120 cm$\times$120 cm, and the distance between the points and lines is 20 cm. A total of 49 points with 735 responses are simulated for the response of three targets. The targets A, B, and C are placed in the positions of (40, 45, $-$60), (80, 45, $-$50), and (60, 75, $-$40), respectively. The characteristic responses of three targets are (15, 1, 1), (10, 1, 1), and (5, 1, 1), respectively. In Figure 6(b), the white noise with the variance 2% the strongest signal amplitude is added to the simulated response of multi-target.

The performance of improved DE algorithm with Gram–Schmidt orthogonalization and position rearrangement is compared with the conventional DE algorithm in terms of the speed of convergence and the accuracy of estimated position and characteristic response. The number of individuals in the population is set to 180, which is 20 times the number of parameters. Convergence of target position with both DE algorithms is shown in Figure 7.

Figure 7 shows that neither DE algorithms fail to achieve the separation of three targets when the iteration progresses to the 25th generation. At the 50th generation, the improved DE algorithm achieves the preliminary classification of the three targets. By the 100th generation, the positions in the population of improved DE algorithm all converge to the preset positions, while the conventional DE algorithm still cannot achieve the effective separation of the three targets. Compared with the conventional DE algorithm, the proposed improved DE algorithm can improve the convergence speed and separate the targets well.

Individual with the smallest cost function is chosen as the optimal solution. The results of 40 inversions of simulated response in Figure 6(b) with two DE algorithms are shown in Figures 8 and 9. The inverted positions and characteristic responses of multi-target by conventional and improved DE algorithms are compared with the true ones. The max generation is set to 100 to terminate the algorithm.

Figure 8 shows that the estimated positions for three targets with conventional and improved DE algorithms consistent well with the true positions. The consistency of the positions estimated by improved DE algorithm is much better than that estimated by conventional DE algorithm. The mean and variance of positions estimated by the conventional and improved DE algorithms are shown in Table 2.

Table 2 shows that the means of estimated positions by the conventional and improved DE algorithms fit well with the true positions. This result indicates both DE algorithms can converge to the true position. However, the variance of the improved DE algorithm is approximately 10% of that of the conventional DE algorithm. That is, the estimated position of the improved DE algorithm has lower fluctuation and higher accuracy.

The estimated characteristic response is shown in Figure 9.

As shown in Figure 9, most of the estimated characteristic responses $l_{\mathrm{v}1}(t)$ and $l_{\mathrm{v}2}(t)$ with both DE algorithms vary greatly from the true ones for the noise. Thus, the estimated characteristic response $l_{\mathrm{v}1}(t)$ and $l_{\mathrm{v}2}(t)$ cannot be used for target reorganization. The estimated characteristic responses $l_{\mathrm{p}}(t)$ for three targets with improved DE algorithm are greatly consistent with the true characteristic response but fluctuate greatly with conventional DE algorithm. The mean and variance of the characteristic response $l_{\mathrm{p}}(t)$ estimated by conventional and improved DE algorithms are shown in Table 3.

The mean of estimated $l_{\mathrm{p}}(t)$ by improved DE algorithm for all targets consistent well with the true one with the maxim error no more than 2% of the true one for target C. The maxim variance is no more than 6% of the $l_{\mathrm{p}}(t)$ for target B. For conventional DE algorithm, the error of mean for estimated $l_{\mathrm{p}}(t)$ reaches 44% and 10% of the true one for targets B and C, respectively. The maxim variance is over 60% of the $l_{\mathrm{p}}(t)$ for target B, and it is 10 times that estimated by the improved DE algorithm.

The conventional DE algorithm can only ensure the smallest overall error of the response but cannot guarantee that each target obtains the best characteristic response. The Gram–Schmidt orthogonalization in the improved DE algorithm enables direct extraction of the best magnetic polarization tensor from the superimposed response. Accordingly, the accuracy of the estimated characteristic response is more than 10 times that of the conventional DE algorithm.

V. FIELD EXPERIMENT AND DISCUSSION

A. DESCRIPTION OF TARGET

The field experiment is conducted in Dalin Town, Tongliao City. The responses of five types of UXOs and five types of harmless targets are measured and inverted with conventional and improved DE algorithms for target location and

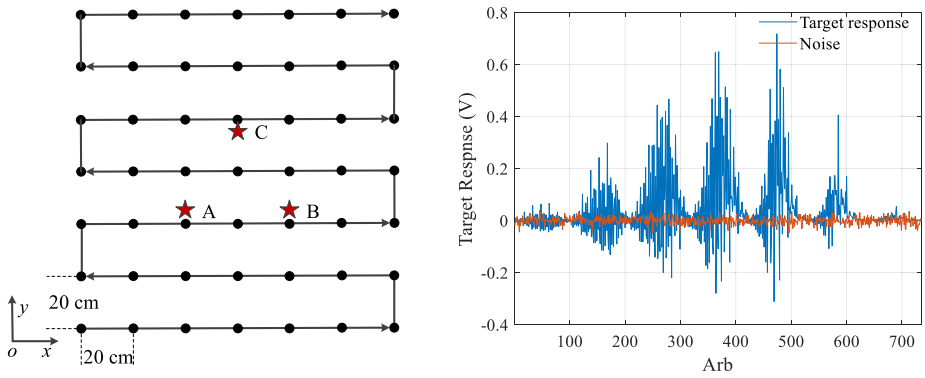

FIGURE 6. (a) Measurement grid for three-target response, (b) simulated response and white noise.

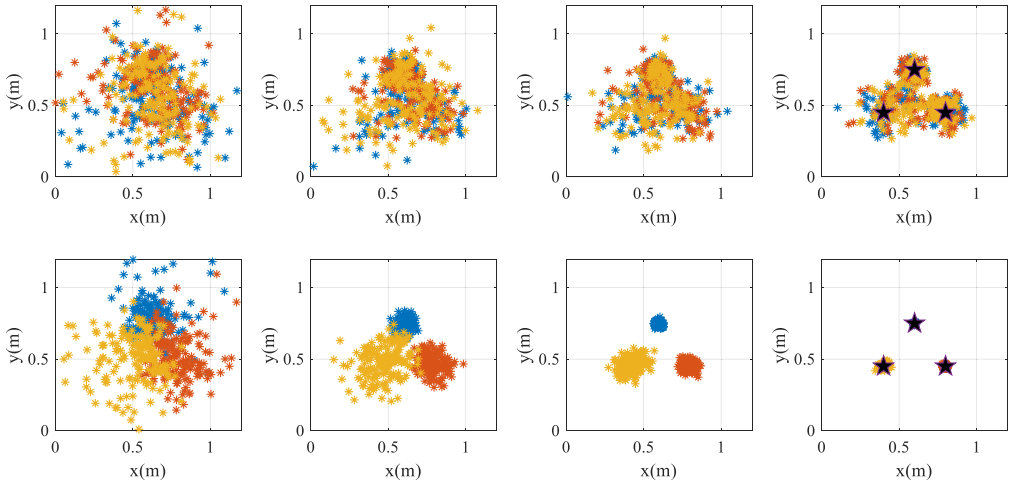

FIGURE 7. Convergence of horizontal positions with both DE algorithms. The four columns represent the estimated positions at the 25th, 50th, 75th, and 100th generations of the DE algorithm. The first line indicates the estimated positions by the conventional DE algorithm. The second line indicates estimated positions by the improved DE algorithm with Gram–Schmidt orthogonalization and position rearrangement. The five-pointed stars in the last two figures represent the true positions of three targets. The three colors refer to positions r_{d1G}, r_{d2G}, and r_{d3G} in the G-th generation, respectively.

TABLE 2. Comparison of estimated position for three targets.

Target	True position (cm)	Conventional DE algorithm		Improved DE algorithm	
		Mean (cm)	Variance (cm)	Mean (cm)	Variance (cm)
A	(40, 45, −60)	(42, 49, −57)	(6.0, 4.2, 3.8)	(39, 49, −56)	(0.75, 0.84, 0.60)
B	(80, 45, −50)	(81, 45, −53)	(2.5, 2.6, 2.5)	(82, 45, −53)	(0.32, 0.41, 0.28)
C	(60, 75, −40)	(61, 74, −41)	(2.0, 1.5, 1.7)	(61, 74, −40)	(0.26, 0.20, 0.21)

TABLE 3. Comparison of estimated characteristic response for three targets.

Target	True $I_p(t)$ (V)	Conventional DE algorithm		Improved DE algorithm	
		Mean (V)	Variance (V)	Mean (V)	Variance (V)
A	15	14.7	4.1	15.0	0.5
B	10	14.4	5.9	10.1	0.6
C	5	5.5	1.3	4.9	0.1

characterization. Table 4 describes the characteristic of these targets in detail.

UXOs in Table 4 are numbered from U1 to U5. The corresponding lengths of these UXOs are from 24 cm to 35 cm, and their outer diameters are from 57 mm to 82 mm. Five types of harmless target, namely, three pipes with an outer diameter of 75 mm and lengths from 10 cm to 30 cm, one three-way connector, and a 64 mm steel ball, are numbered from O1 to O5.

All these targets are buried in groups of two or three. Same as in simulated experiment, the measurement area of field experiment is set to 120 cm×120 cm with 20 cm distance

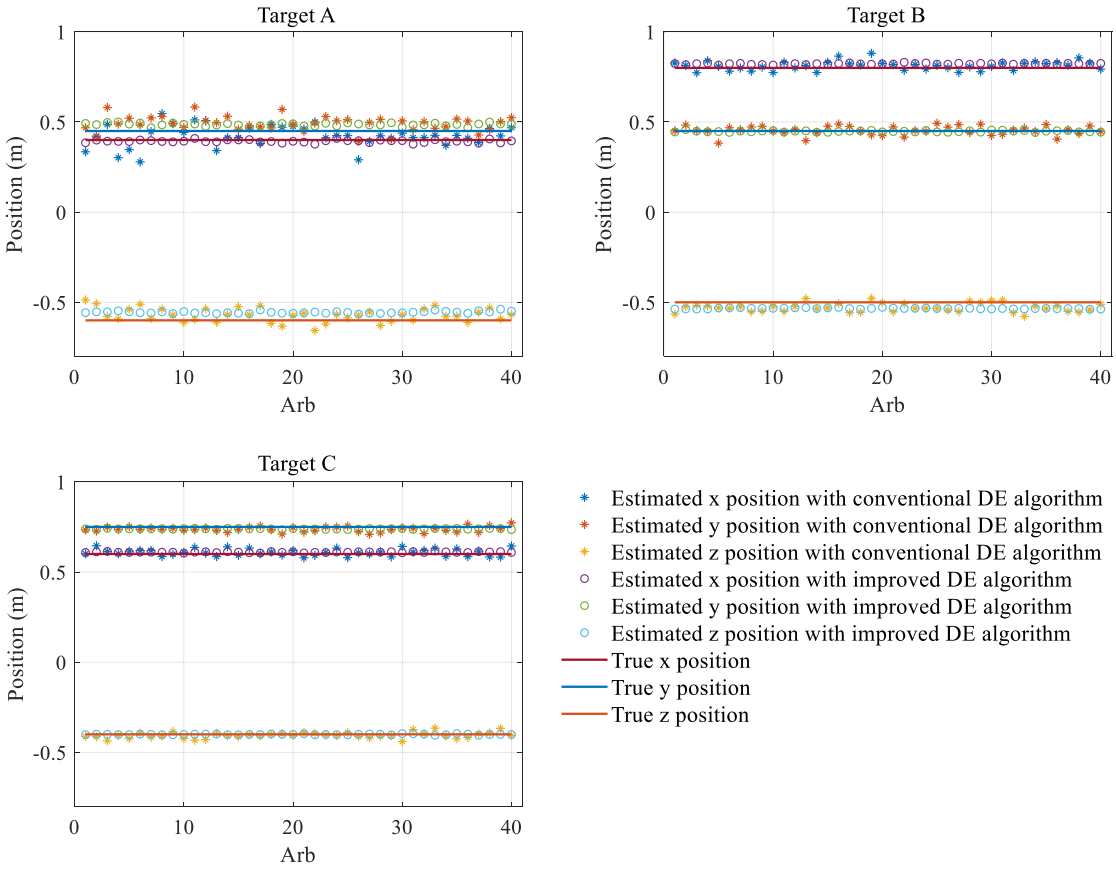

FIGURE 8. Comparison of estimated positions for three targets by two algorithms.

TABLE 4. Target description.

Number	Length (cm)	Diameter (mm)	Number	Picture
U1	24	60	3	
U2	26	57	1	
U3	27	82	1	
U4	34	75	1	
U5	35	74	1	
O1	30	75	1	
O2	20	75	1	
O3	10	75	1	
O4	12.5	/	1	
O5	/	64	1	

from each point. A total of 49 points with 735 responses are measured for every measurement. All measurements in the field experiment use 40 channels from 0.2 ms to 20 ms. Given 50 repetitions for a measurement duration of 4 s per data point, the signal noise ratio (SNR) of the response can be greatly improved. In the next section, the responses of two and three targets are inverted by conventional and improved DE algorithms to locate and characterize every target.

TABLE 5. Variance of estimated target position by two algorithms.

Target	O2 (cm)	U1 (cm)	O4 (cm)
Conventional DE algorithm	(5.5, 13.6, 4.0)	(7.4, 11.2,3.6)	(6.3, 7.4, 6.1)
Improved DE algorithm	(3.2, 1.8, 0.55)	(0.76, 4.0, 1.3)	(2.3, 1.7, 1.2)

B. COMPARATION OF TWO ALGORITHMS

Different from the DE algorithm in the simulated experiment, that in field experiment it needs to process 40 channels of data from 0.2 ms to 20 ms.

First, response of three targets U1, O2, and O4 buried at (60.0, 75.0, −51.0), (40.0, 45.0, −44.0), and (80.0, 45.0, −47.7), with inclination of 90°, 0°, and 0°, respectively, is inverted with conventional and improved DE algorithms for every time channel to compare the performance of the two algorithms. The results are shown in Figures 10 and 11.

Figure 10 shows that the conventional and improved DE algorithms can estimate the target position well based on the early response with high SNR. As the SNR of target response decreases, the estimated position of target differs greatly from the true position. The estimated positions with conventional DE algorithm differ from channel to channel, while the estimated positions with improved DE algorithm have higher consistency. The variances of the estimated positions from

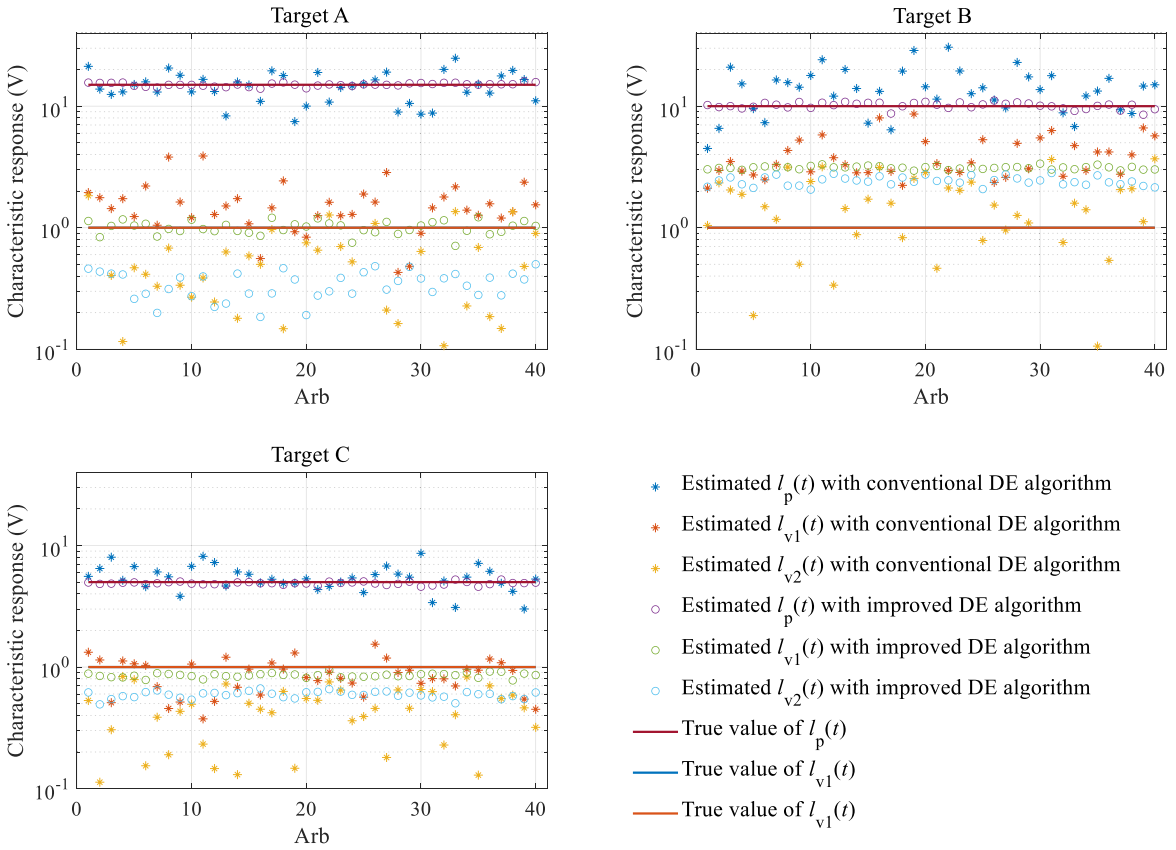

FIGURE 9. Comparison of estimated characteristic response for three targets by two algorithms.

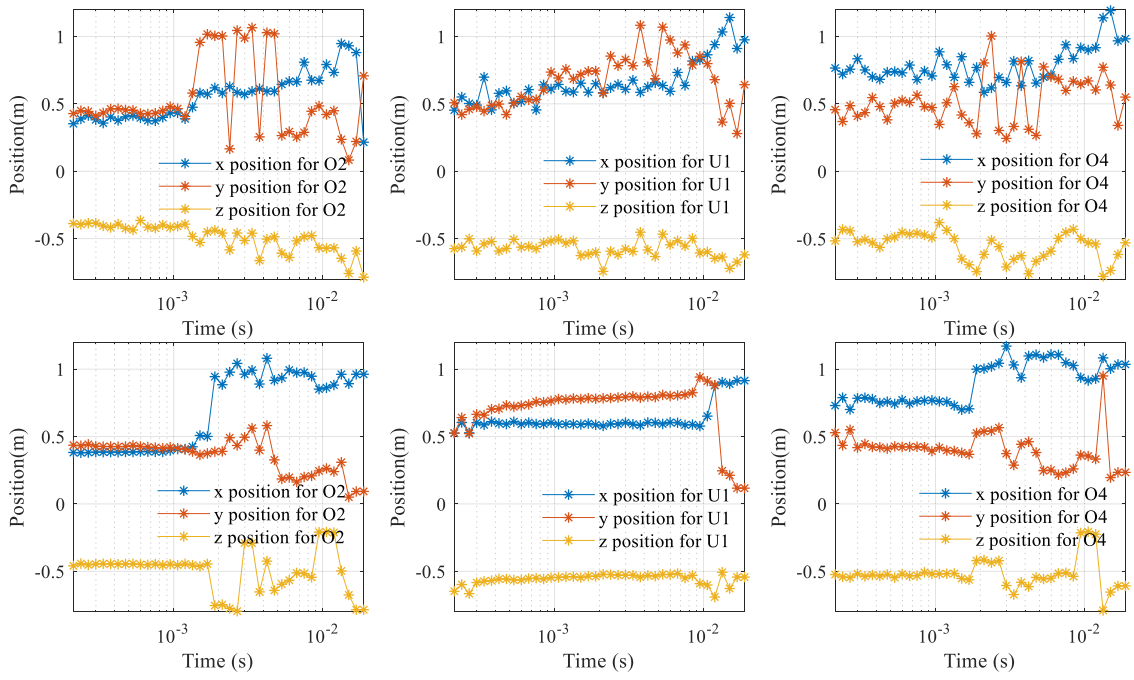

FIGURE 10. Estimated positions for each target with two DE algorithms. Figures in line 1 refer to the estimated positions with conventional DE algorithm. Figures in line 2 refer to the estimated positions with improved DE algorithm.

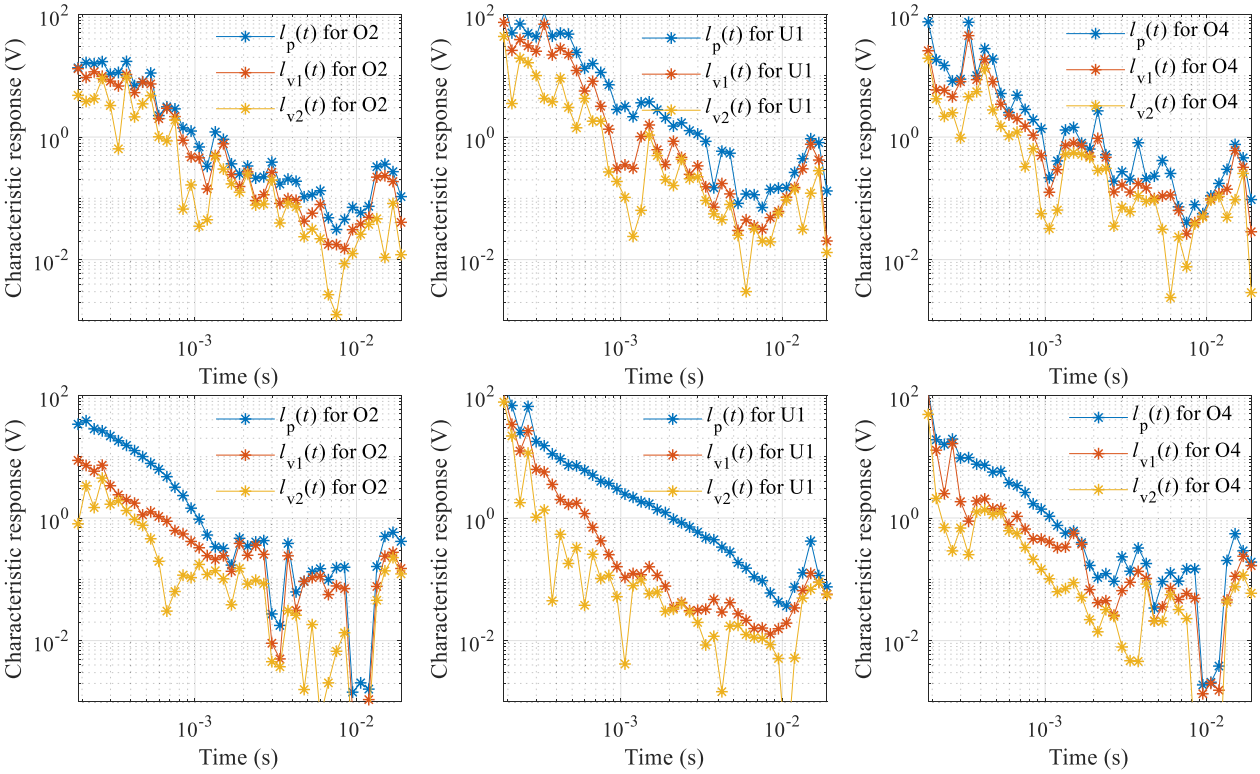

FIGURE 11. Estimated characteristic responses for each target with two DE algorithms. Figures in line 1 refer to the estimated characteristic responses with conventional DE algorithm. Figures in line 2 refer to the estimated characteristic responses with improved DE algorithm.

TABLE 6. Positions of multiple targets.

Groups	Targets	True positions (cm)	True inclination (°)	Estimated positions (cm)	Errors (cm)
1	U1	(40.0, 60.0, −42.2)	0	(41.1, 58.8, −45.2)	(1.1, −1.2, −3.0)
	U1	(80.0, 60.0, −43.6)	0	(79.7, 60.8, −42.8)	(−0.3, 0.8, 0.8)
2	U1	(40.0, 60.0, −44.2)	0	(42.2, 58.5, −46.1)	(2.2, −1.5, −1.9)
	U2	(80.0, 60.0, −41.8)	0	(78.0, 60.2, −41.0)	(−2.0, 0.2, 0.8)
3	U2	(40.0, 60.0, −41.0)	0	(41.3, 59.0, −41.5)	(1.3, −1.0, −0.5)
	U3	(80.0, 60.0, −43.7)	0	(79.2, 60.0, −38.9)	(−0.8, 0.0, 4.8)
4	U3	(40.0, 60.0, −50.1)	45	(35.4, 63.9, −49.8)	(−4.6, 3.9, 0.3)
	O4	(80.0, 60.0, −47.8)	/	(74.3, 63.1, −51.3)	(−5.7, 3.1, −3.5)
5	U4	(40.0, 60.0, −51.3)	90	(37.3, 58.0, −56.9)	(−2.7, −2.0, −5.6)
	O1	(80.0, 60.0, −51.3)	90	(74.3, 68.0, −54.6)	(−5.7, −2, −3.3)
6	O3	(40.0, 60.0, −40.3)	90	(41.5, 61.3, −42.6)	(1.5, 1.3, −2.3)
	O5	(80.0, 60.0, −40.8)	/	(79.6, 61.6, −46.4)	(−0.4, 1.6, −5.6)
7	U1	(60.0, 75.0, −42.0)	0	(60.8, 76.4, −43.9)	(0.8, 1.4, -1.9)
	U1	(40.0, 45.0, −42.0)	0	(41.1, 43.5, −41.8)	(1.1, −1.5, 0.2)
	U1	(80.0, 45.0, -51.0)	90	(80.1, 36.0, -51.3)	(0.1, −9.0, −0.3)
8	U1	(60.0, 75.0, −41.0)	90	(56.3, 75.0, −47.9)	(−3.7, 0.0, −6.9)
	U2	(40.0, 45.0, −40.9)	90	(41.8, 49.0, −47.6)	(1.8, 4.0, −6.7)
	U3	(80.0, 45.0, −39.9)	90	(75.2, 46.9, −45.1)	(−4.8, 1.9, −5.2)
9	U3	(60.0, 75.0, −49.4)	90	(65.4, 67.4, −51.7)	(5.4, −7.6, −2.3)
	U5	(40.0, 45.0, −50.3)	90	(40.6, 46.6, −55.4)	(0.6, 1.6, −5.1)
	O1	(80.0, 45.0, −39.0)	0	(80.4, 45.1, −32.9)	(0.4, 0.1, 6.1)

0.283 ms to 1.416 ms with two algorithms are compared, and the results are shown in Table 5.

In Table 5 , the estimated position by the improved DE algorithm is more consistent, and the variance is mostly between 1.0 and 2.0 cm. The variance of estimated position by the conventional DE algorithm is mostly between 5.0 and 10.0 cm, which is nearly five times that of the improved DE algorithm.

Figure 11 shows that the conventional DE algorithm cannot accurately estimate the characteristic responses of the target even for the high SNR response at early time. The improved DE algorithm can accurately estimate the charac-

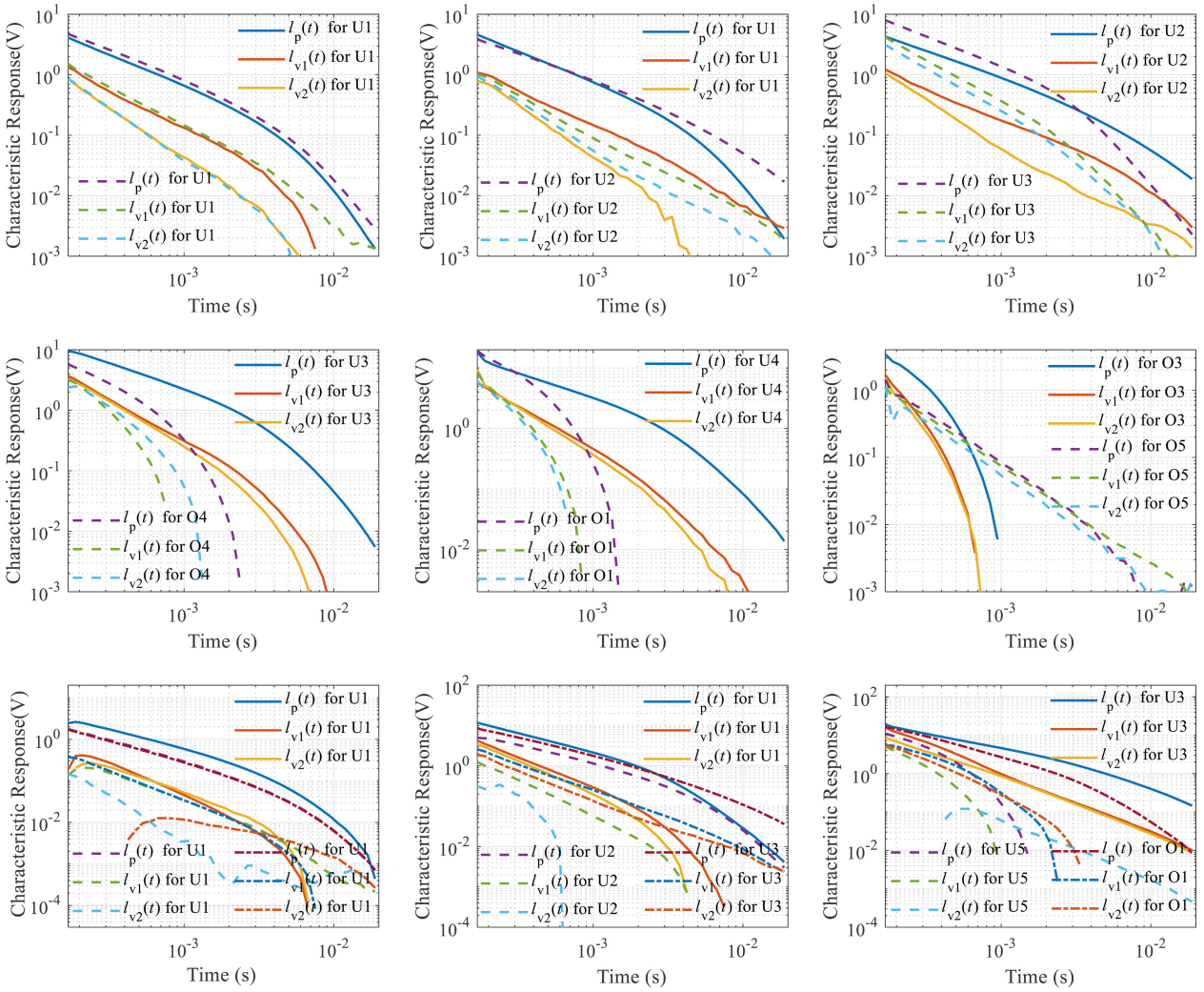

FIGURE 12. Inverted characteristic response for multiple targets.

teristic response $l_p(t)$ of the target for the response of high SNR in the early time. However, it cannot estimate the characteristic responses $l_{v1}(t)$ and $l_{v2}(t)$ of the target. The estimated characteristic response $l_p(t)$ by improved DE algorithm is affected by noise at late time.

C. MULTI-TARGET INVERSION

The accuracy and efficiency of improved DE algorithm can be further optimized by superimposing the early time response with high SNR. The process of improved DE algorithm can be divided into three steps.

Step 1: Average the early time response between 0.2 and 2.0 ms to further improve the SNR of response.

Step 2: Locate the targets by improved DE algorithm with the averaged response.

Step 3: Estimate the characteristic responses for every time channel from 0.2 ms to 20.0 ms depending on the estimated position.

On the basis of this process, the improved DE algorithm only estimates the target position once based on the averaged response. This way greatly improves the inversion efficiency. Inversion on six groups of double-target response and three groups of triple-target response is performed to estimate target position and characteristic response. The results are shown in Table 6 and Figure 12.

In Table 6, the positions estimated by the improved DE algorithm are greatly consistent with the true ones for all targets. When the target is vertically orientated, the error of the estimated position in the horizontal direction is very low with mostly 2–3 cm. When the target is flat-lying oriented, the error of estimated position in horizontal direction can be up to 5–9 cm. The reason is that the geometric center of the target does not coincide with the equivalent dipole. When the target is flat-lying oriented, the estimated depth is deeper than the true depth to 3–6 cm, such as U4 and O1 in the 5th group and U1, U2, and U3 in the 8th group. These errors should be given enough attention when locating the target for

excavation. A reasonable pre-judgment on the scope for the excavation should also be conducted.

In Figure 12, the estimated characteristic response of the UXO $l_p(t)$ by the improved DE algorithm has a very high SNR in the early and late times. The SNRs of estimated characteristic response $l_{v1}(t)$, $l_{v2}(t)$ are also high, but they are not consistent. Therefore, target recognition should be based on the characteristic response $l_p(t)$. The amplitude of characteristic response of the harmless target is similar to that of the UXO in the early time but decays much faster, which results in a difference of 2–3 orders of magnitude after 2 ms. Thus, the classification of the underground target should be based on the late time response.

In general, the proposed improved DE algorithm can efficiently and accurately estimate the target position and characteristic response even if these target responses are superimposed.

VI. CONCLUSION

An improved DE algorithm with Gram–Schmidt orthogonalization and position rearrangement based on multisource model is proposed to locate and characterize multiple targets from the superimposed response measured by a portable TEM sensor.

The Gram–Schmidt orthogonalization turns the coefficient matrix into an orthonormal basis. This way enables direct extraction of the magnetic polarization tensor from the superimposed response. Positions of individuals in the contemporary population are divided into different groups belonging to different targets. Thus, crossover operation can be performed within the group, which greatly accelerates the convergence of DE algorithm.

Simulated superimposed response is inverted 40 times by conventional and improved DE algorithms to analyze the performance. The results show that the convergence of the algorithm can be effectively accelerated by the position rearrangement. The variance of position and characteristic response estimated by the improved DE algorithm is only 10% of that of the conventional DE algorithm. The error of estimated characteristic response $l_p(t)$ with improved DE algorithm is no more than 20% of that by the conventional DE algorithm. Overall, the performance of DE algorithm is greatly improved by Gram–Schmidt orthogonalization and position rearrangement.

Field experiment is conducted to compare the performance of two algorithms, and its results show that the variance of estimated positions in different time channels by the improved DE algorithm is mostly between 1.0 and 2.0 cm. This value is only 20% of that of the conventional DE algorithm. Only the improved DE algorithm can accurately estimate the characteristic response $l_p(t)$ from superimposed response with high SNR at early time. The inversion efficiency and accuracy are greatly improved as evidenced by the averaged response. The estimated characteristic response $l_p(t)$ has a very high SNR throughout the time for UXOs. This result verifies the performance of the improved DE algorithm.

REFERENCES

[1] O. O. Bilukha, M. Brennan, and M. Anderson, "Injuries and deaths from Landmines and unexploded ordnance in Afghanistan, 2002-2006," *JAMA J. Amer. Med. Assoc.*, vol. 298, no. 5, pp. 516–518, 2007.
[2] C. Chirgwin, "Managing land mine and UXO contamination in exploration projects," *Lead. Edge*, vol. 24, no. 4, pp. 376–377, Apr. 2005.
[3] P. B. Weichman, "Validation of advanced EM models for UXO discrimination," *IEEE Trans. Geosci. Remote Sens.*, vol. 51, no. 7, pp. 3954–3967, Jul. 2013.
[4] L. Beran, B. Zelt, and S. Billings, "Detecting and classifying UXO," *J. Conventional Weapons Destruction*, vol. 17, no. 1, p. 15, 2015.
[5] D. K. Butler, H. H. Bennett, and J. H. Ballard, "Overview of multimethod geophysical system development for enhanced near-surface target detection, discrimination, and characterization," *Lead. Edge*, vol. 25, no. 3, pp. 352–356, 2006.
[6] S. D. Billings, "Discrimination and classification of buried unexploded ordnance using magnetometry," *IEEE Trans. Geosci. Remote Sens.*, vol. 42, no. 6, pp. 1241–1251, Jun. 2004.
[7] W. E. Doll, J. R. Sheehan, T. J. Gamey, L. P. Beard, and J. Norton, "Results of an airborne vertical magnetic gradient demonstration, new mexico," *J. Environ. Eng. Geophys.*, vol. 13, no. 3, pp. 277–290, Sep. 2008.
[8] Q. Xiaodong, W. Chen, F. Guangyou, and Y. Hejun, "Detecting anomaly targets using handheld frequency domain electromagnetic system," *Sens. Actuators A, Phys.*, vol. 268, pp. 155–163, Dec. 2017.
[9] T. Bell, B. Barrow, J. Miller, and D. Keiswetter, "Time and frequency domain electromagnetic induction signatures of unexploded ordnance," *Subsurf. Sens. Technol. Appl.*, vol. 2, no. 3, pp. 153–175, 2001.
[10] C.-C. Chen, M. B. Higgins, K. O'Neill, and R. Detsch, "Ultrawide-bandwidth fully-polarimetric ground penetrating radar classification of subsurface unexploded ordnance," *IEEE Trans. Geosci. Remote Sens.*, vol. 39, no. 6, pp. 1221–1230, Jun. 2001.
[11] X. Núñez-Nieto, M. Solla, P. Gómez-Pérez, and H. Lorenzo, "Signal-to-Noise ratio dependence on ground penetrating radar antenna frequency in the field of landmine and UXO detection," *Measurement*, vol. 73, pp. 24–32, Sep. 2015.
[12] X. Núñez-Nieto, M. Solla, P. Gómez-Pérez, and H. Lorenzo, "GPR signal characterization for automated landmine and UXO detection based on machine learning techniques," *Remote Sens.*, vol. 6, no. 10, pp. 9729–9748, Oct. 2014.
[13] T. Ahmed, Z. Xiaofei, and Z. Wang, "DOA estimation for coprime EMVS arrays via minimum distance criterion based on PARAFAC analysis," *IET Radar, Sonar Navigat.*, vol. 13, no. 1, pp. 65–73, Jan. 2019.
[14] F. Wen, J. Shi, and Z. Zhang, "Joint 2D-DOD, 2D-DOA and polarization angles estimation for Bistatic EMVS-MIMO radar via PARAFAC analysis," *IEEE Trans. Veh. Technol.*, vol. 69, no. 2, pp. 1626–1638, Feb. 2020.
[15] F. Wen and J. Shi, "Fast direction finding for bistatic EMVS-MIMO radar without pairing," *Signal Process.*, vol. 173, Aug. 2020, Art. no. 107512.
[16] J. S. Holladay, W. E. Doll, L. P. Beard, J. L. C. Lee, and D. T. Bell, "UXO time-constant estimation from helicopter-borne TEM data," *J. Environ. Eng. Geophys.*, vol. 11, no. 1, pp. 43–52, Mar. 2006.
[17] M. Prouty, D. C. George, and D. D. Snyder, *MetalMapper: A Multi-Sensor TEM System for UXO Detection and Classification*. San Jose, CA, USA: Geometrics, 2011.
[18] E. Gasperikova, J. Smith, H. Morrison, and A. Becker, "UXO detection and identification based on intrinsic target polarizabilities—A case history," *Geophysics*, vol. 74, no. 1, pp. B1–B8, 2008.
[19] D. A. Steinhurst, "EMI array for cued UXO discrimination," Environ. Secur. Technol. Certification Program Office (DOD) Arlington, VA, USA, Tech. Rep. ESTCP-PR-MM-0601, 2010.
[20] J. P. Fernandez, B. E. Barrowes, T. M. Grzegorczyk, N. Lhomme, K. O'Neill, and F. Shubitidze, "A man-portable vector sensor for identification of unexploded ordnance," *IEEE Sensors J.*, vol. 11, no. 10, pp. 2542–2555, Oct. 2011.
[21] J. Fernandez, "MPV-II: An enhanced vector man-portable EMI sensor for UXO identification," *Proc. SPIE Int. Soc. Opt. Photon.*, vol. 8017, May 2011, Art. no. 801707.
[22] H. Wang, S. Chen, S. Zhang, Z. Yuan, H. Zhang, D. Fang, and J. Zhu, "A high-performance portable transient electro-magnetic sensor for unexploded ordnance detection," *Sensors*, vol. 17, no. 11, p. 2651, Nov. 2017.
[23] S. Chen, S. Zhang, H. Jiang, and J. Zhu, "Location and characterization of unexploded ordnance-like targets with a portable transient electromagnetic system," *IEEE Access*, vol. 8, pp. 150174–150185, 2020.

[24] Y. Zhang, L. Collins, H. Yu, C. E. Baum, and L. Carin, "Sensing of unexploded ordnance with magnetometer and induction data: Theory and signal processing," *IEEE Trans. Geosci. Remote Sens.*, vol. 41, no. 5, pp. 1005–1015, May 2003.
[25] A. Tarokh, E. Miller, I. Won, and H. Huang, "Statistical classification of buried objects from spatially sampled time or frequency domain electromagnetic induction data," *Radio Sci.*, vol. 39, no. 4, pp. 1–11, 2004.
[26] A. Aliamiri, J. Stalnaker, and E. L. Miller, "Statistical classification of buried unexploded ordnance using nonparametric prior models," *IEEE Trans. Geosci. Remote Sens.*, vol. 45, no. 9, pp. 2794–2806, Sep. 2007.
[27] Q. Liu, X. Liao, and L. Carin, "Detection of unexploded ordnance via efficient semisupervised and active learning," *IEEE Trans. Geosci. Remote Sens.*, vol. 46, no. 9, pp. 2558–2567, Sep. 2008.
[28] S. Chen, S. Zhang, J. Zhu, and X. Luan, "Accurate measurement of characteristic response for unexploded ordnance with transient electromagnetic system," *IEEE Trans. Instrum. Meas.*, vol. 69, no. 4, pp. 1728–1736, Apr. 2020.
[29] F. Shubitidze, J. P. Fernández, I. Shamatava, B. E. Barrowes, and K. O'Neill, "Joint diagonalization applied to the detection and discrimination of unexploded ordnance," *Geophysics*, vol. 77, no. 4, pp. WB149–WB160, Jul. 2012.
[30] F. Shubitidze, "A complex approach to UXO discrimination: Combining advanced EMI forward models and statistical signal processing," Sky Res., Ashland, OR, USA, Tech. Rep. SERDP Project MR-1572, 2012.
[31] F. Shubitidze, J. P. Fernandez, B. E. Barrowes, I. Shamatava, A. Bijamov, K. O'Neill, and D. Karkashadze, "The orthonormalized volume magnetic source model for discrimination of unexploded ordnance," *IEEE Trans. Geosci. Remote Sens.*, vol. 52, no. 8, pp. 4658–4670, Aug. 2014.
[32] F. Shubitidze, "The ortho normalized vol. magnetic, source technique applied to live-site uxo data: Inversion and classification studies," in *Proc. SEG Tech. Program Expanded Abstr. Soc. Explor. Geophys.*, Jan. 2011, pp. 3766–3770.
[33] L.-P. Song, D. W. Oldenburg, and L. R. Pasion, "Estimating source locations of unexploded ordnance using the multiple signal classification algorithm," *Geophysics*, vol. 77, no. 4, pp. WB127–WB135, Jul. 2012.
[34] D. P. Economou, F. Shubitidze, B. Barrowes, and N. K. Uzunoglu, "MUSIC algorithm applied to advanced EMI sensors data for UXO classification," in *Proc. Int. Conf. Electromagn. Adv. Appl.*, Sep. 2011, pp. 1160–1163.
[35] L.-P. Song, L. R. Pasion, S. D. Billings, and D. W. Oldenburg, "Nonlinear inversion for multiple objects in transient electromagnetic induction sensing of unexploded ordnance: Technique and applications," *IEEE Trans. Geosci. Remote Sens.*, vol. 49, no. 10, pp. 4007–4020, Oct. 2011.
[36] J. T. Miller, "Source separation using sparse-solution linear solvers," *Proc. SPIE Int. Soc. Opt. Photon.* vol. 7664, Apr. 2010, Art. no. 766409.
[37] Song, Lin-Ping, "Transient electromagnetic inversion for multiple targets," *Proc. SPIE Int. Soc. Opt. Photon.*, vol. 7303, May 2009, Art. no. 73030R.
[38] R. Storn and K. Price, "Differential evolution-a simple and efficient heuristic for global optimization over continuous spaces," *J. Global Optim.*, vol. 1997, vol. 11, no. 4, pp. 341–359.

SHUDONG CHEN received the B.Sc. degree in biomedical engineering, the M.Sc. degree in circuits and systems, and the Ph.D. degree in instrument science and technology from Jilin University, Jilin, China, in 2007, 2009, and 2012, respectively. He has developed portable and vehicle transient electromagnetic systems for detecting landmines and unexploded ordnance. He also studies the detection and recognition theory of these targets. He is currently an Associate Professor with the College of Electronic Science and Engineering, Jilin University. His current research interests include weak signal detection, electromagnetic detection theory, and system design.

SHUANG ZHANG received the Ph.D. degree in circuits and systems from Jilin University, Jilin, China, in 2008. He has developed land and marine proton precession magnetic sensor based on prepolarization and dynamic nuclear polarization effect for weak magnetic detection, detecting landmines, and unexploded ordnance. He also studies the design and optimization of EMI system for unexploded ordnance detection. He is currently a Professor with the College of Electronic Science and Engineering, Jilin University. His current research interests include weak signal detection, electromagnetic detection theory, and system design.

XINQUN LUAN is currently a Senior Engineer with the Science and Technology on Near-Surface Detection Laboratory, Wuxi, China. Her current research interest includes near surface detection technology.

ZHAOHE LIU is currently an Engineer with the Science and Technology on Near-Surface Detection Laboratory, Wuxi, China. His current research interest includes near surface detection technology.